Nanoscale Research Letters

NANO EXPRESS

Open Access

# Study of Thermometry in Two-Dimensional $Sb_2Te_3$ from Temperature-Dependent Raman Spectroscopy

Manavendra P. Singh[1†], Manab Mandal[2†], K. Sethupathi[2], M. S. Ramachandra Rao[1,3] and Pramoda K. Nayak[1*]

**Abstract**

Discovery of two-dimensional (2D) topological insulators (TIs) demonstrates tremendous potential in the field of thermoelectric since the last decade. Here, we have synthesized 2D TI, $Sb_2Te_3$ of various thicknesses in the range 65–400 nm using mechanical exfoliation and studied temperature coefficient in the range 100–300 K using micro-Raman spectroscopy. The temperature dependence of the peak position and line width of phonon modes have been analyzed to determine the temperature coefficient, which is found to be in the order of $10^{-2}$ $cm^{-1}$/K, and it decreases with a decrease in $Sb_2Te_3$ thickness. Such low-temperature coefficient would favor to achieve a high figure of merit (*ZT*) and pave the way to use this material as an excellent candidate for thermoelectric materials. We have estimated the thermal conductivity of $Sb_2Te_3$ flake with the thickness of 115 nm supported on 300-nm $SiO_2$/Si substrate which is found to be ~ 10 W/m–K. The slightly higher thermal conductivity value suggests that the supporting substrate significantly affects the heat dissipation of the $Sb_2Te_3$ flake.

**Keywords:** Thermometry, Topological insulators, Thermoelectric, Micro-Raman, Figure of merit, Thermal conductivity

## Introduction

Topological insulators (TIs) are the new class of quantum materials having a wide energy gap in the bulk and surface gap less Dirac-like states, which are protected under time-reversal symmetry [1–3]. These materials hold great promise for a broad range of potential applications, including field-effect transistors [4, 5], infrared-THz detectors [6], magnetic field sensors [7, 8] and thermoelectricity [9, 10]. The thermoelectric performance of any material at a temperature $T$ is governed by the dimensionless figure of merit $ZT$ ($ZT = S^2\sigma T/\kappa$, where $S$, $\sigma$ and $\kappa$ denote the Seebeck coefficient, electrical conductivity and thermal conductivity, respectively [11, 12]. Reduced dimensionality of these materials has been proven to be one of the most common approaches to minimize the thermal conductivity and to obtain high $ZT$ [13]. To minimize the thermal conductivity, it is very important to understand the phonon dynamics in this type of material, particularly the phonon–phonon and electron–phonon interactions, all of which have a great impact on the thermoelectric device performance [14, 15].

Raman scattering has been proved as an important tool for probing the vibrational modes in a material based on its non-destructive and microscopic nature [16, 17]. It also provides important information on doping, strain engineering and crystal phases [18, 19]. While the room-temperature Raman characterizations of phonon modes in various 2D TIs have been well studied in the literature [20, 21], temperature dependence Raman characterizations are still in the nascent stage. Furthermore, it is well known that change of temperature can vary inter-atomic distances and affect various phonon modes in the crystal [14]. Therefore, temperature-dependent Raman spectra are well suitable to obtain information on the thermal

*Correspondence: pnayak@iitm.ac.in
†Manavendra P. Singh and Manab Mandal have contributed equally to this work
[1] Department of Physics and Materials Science Research Centre, Indian Institute of Technology Madras, Chennai 600 036, India
Full list of author information is available at the end of the article

conductivity of materials, as well as isotopic effects and phonon lifetimes [22, 23].

In this work, we present power-dependent Raman spectroscopy at room temperature and temperature-dependent Raman spectroscopy in the temperature range between 100 and 300 K of 2D $Sb_2Te_3$ crystals of various thicknesses. The variation of Raman peak position and full width at half maximum (*FWHM*) with respect to temperature and power have been analyzed, and the results are interpreted to determine the thermal expansion coefficient and thermal conductivity of $Sb_2Te_3$ flakes in the context of thermometry study. The value of thermal conductivity for $Sb_2Te_3$ flake with a thickness of 115 nm has been estimated, and the role of the substrate to enhance the thermal conductivity has been discussed.

## Methods

Mechanical exfoliation was carried out on high-quality bulk $Sb_2Te_3$ crystal (2D Semiconductors, USA) using standard scotch tape technique [24] to obtain $Sb_2Te_3$ flakes of different thickness (65 nm, 80 nm, 115 nm, 200 nm and 400 nm) on 300-nm $SiO_2$/Si substrates. Exfoliated samples were identified with the help of an optical microscope (LV100ND- Nikon Microscope). The lateral sizes of the $Sb_2Te_3$ nanoflakes are found in the range of 5–7 μm. Park NX-10 AFM (atomic force microscopy) was used to measure the thickness of the $Sb_2Te_3$ flakes using non-contact mode.

The Raman spectra were measured on various flakes using a HORIBA LabRAM confocal micro-Raman system in a backscattering geometry using a 632-nm laser excitation. A laser with spot size ~ 1 μm and tunable optical power from ~ 0.4 to 2.6 mW was used as the excitation source. The spectra were collected using a spectrometer equipped with a liquid-nitrogen-cooled CCD camera. The spectra were acquired in the frequency range from 100 to 200 $cm^{-1}$ with a spectral resolution of 1 $cm^{-1}$. All the measurements were taken using an integration time of 10 s, acquisitions of 10, and 1800 grating. For room temperature (RT) measurements, 100 × objective was used, while long working distance 50 × objective was used for low-temperature measurements.

## Results and Discussion

$Sb_2Te_3$ is a TI, which crystallizes in the rhombohedral crystal structure with space group $D^5_{3d}(R\bar{3}m)$, and its unit cell contains five atoms [20]. This crystal is formed by stacking five-atom layers along the *z*-direction, which is known as a quintuple layer (QL) as shown in Fig. 1, with a thickness of about 0.96 nm [20]. From the atomic registry, we can see that the Sb atom is sandwiched between two Te atoms, with the $Te^{(2)}$ atom acting as an inversion centre. This centrosymmetric property of the crystal structure gives rise to mutually independent Raman active modes. The atoms within a single QL are held together by strong covalent forces, while the force between QLs is much weaker and of van der Waal's type. Due to weak van der Waal force in the out-of-plane direction, it is possible to mechanically exfoliate thin layers of this material from its bulk crystals. Although exfoliated samples retain the composition and structure of bulk crystals, there is a change in phonon dynamics, when its thickness is reduced to the nanoscale level [25, 26].

Optical micrograph (OM) images of three different $Sb_2Te_3$ nanoflakes exfoliated on $SiO_2$/Si substrate are shown in Fig. 2a-c. The lateral sizes of the flakes are in the range of 5–7 μm, which are large enough to be observed in OM. One can observe that the color contrast of the flakes is very sensitive to the thickness of the flakes *i.e.,* different thicknesses show different color contrast. The thicknesses of these prepared flakes were measured by atomic force microscopy (AFM), which are displayed in the lower panel of Fig. 2 along with their cross-sectional height profiles (Fig. 2d–f). The thickness values of these flakes were estimated to be 65 nm, 115 nm and 200 nm and were found to be almost uniform except for some bumps. But, all the Raman measurements were taken on the position of the flakes, where uniformity was maintained.

Figure 3 presents the power-dependent Raman spectra of above three flakes measured at room temperature, which consists of four vibrational modes including two Raman active modes $E^2_g$ and $A^2_{1g}$ assigned at frequencies ~ 125 $cm^{-1}$ and ~ 169 $cm^{-1}$, and two IR active modes $A^2_{2u}$ and $A^3_{2u}$ assigned at ~ 115 $cm^{-1}$ and ~ 144 $cm^{-1}$, respectively [20, 27]. It is clearly observed that there is a red shift as well as an increase in the peak intensity of all the Raman modes with increase in laser power for all the flakes (65 nm, 115 nm and 200 nm). These changes suggest that the increase in laser power leads to a considerable increase in the local temperature on the surface of the sample [28]. $Sb_2Te_3$ flakes with the thicknesses of 115 nm and 200 nm exhibit all the four modes ($A^2_{2u}$, $E^2_g$, $A^3_{2u}$ and $A^2_{1g}$) for low laser power of 0.402 mW, and $A^2_{2u}$ and $E^2_g$ modes are merged together with further increase in power, which can be seen from the asymmetric line width of $A^2_{2u}/E^2_g$ modes in Fig. 3b, c. Figure 3a shows Raman spectra of $Sb_2Te_3$ flake with a thickness of 65 nm at three different incident laser powers, and the entire spectra exhibit only two Raman modes $E^2_g$ and $A^3_{2u}$ at room temperature. In this case, the shape of $E^2_g$ peaks for all laser powers looks asymmetry, which implies that there is also merging of both $A^2_{2u}$ and $E^2_g$ modes similar to thick flakes (115 nm, 200 nm) at high laser power. However, the $A^2_{1g}$ is completely absent for this thickness. We believe that this mode would be the characteristics of

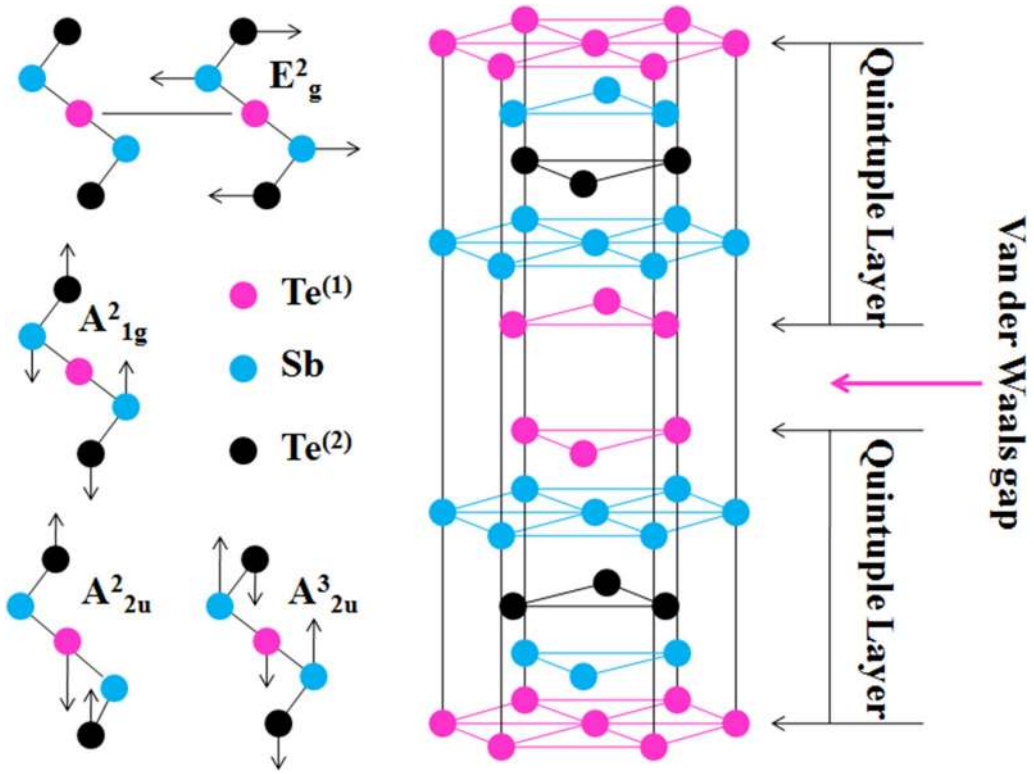


**Fig. 1** Schematic of $Sb_2Te_3$ crystal showing the arrangement of atoms and van der Waals gap. The pink, light blue and black circles represent the $Te^{(1)}$, Sb and $Te^{(2)}$ atoms, respectively. The left panel shows the possible phonon modes in the frequency range 100 $cm^{-1}$ to 200 $cm^{-1}$. The arrows represent direction of vibrations of constituent atoms

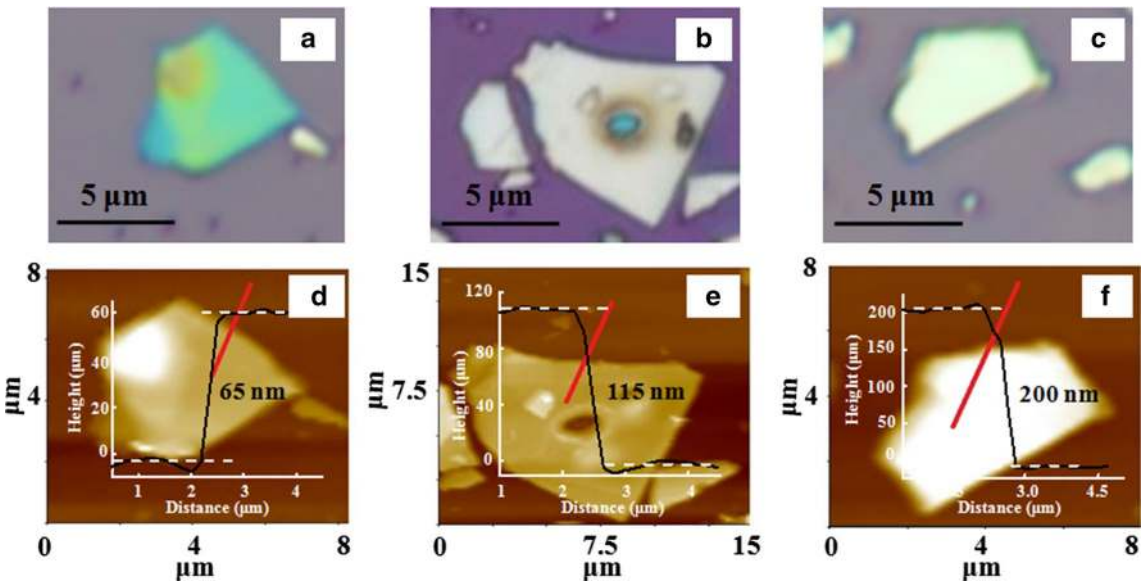


**Fig. 2** **a-c** OM images of $Sb_2Te_3$ flakes of thicknesses of 65 nm, 115 nm and 200 nm, respectively. **d-f** Their representative AFM images and height profiles.

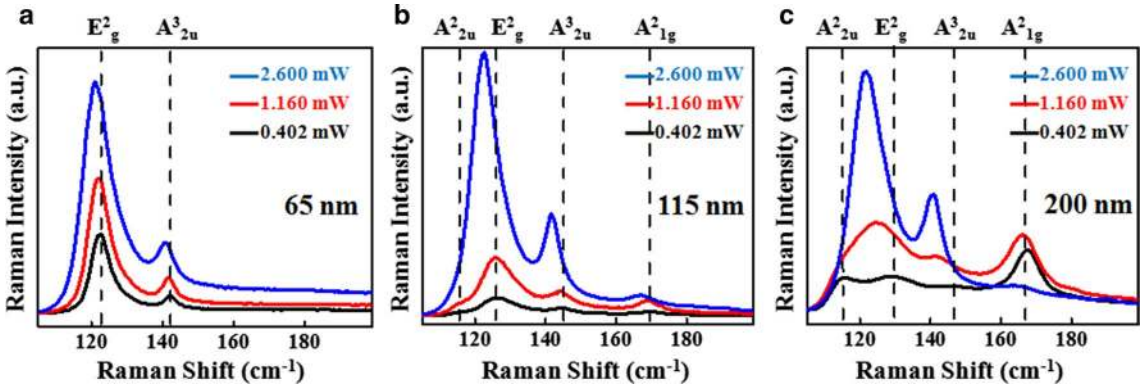


**Fig. 3** **a-c** Power-dependent micro-Raman spectra of 65-nm, 115-nm and 200-nm $Sb_2Te_3$flakes, respectively. The spectra are measured using 632-nm laser with three different powers 0.402 mW, 1.160 mW and 2.600 mW. The dashed lines show the position of the Raman modes.

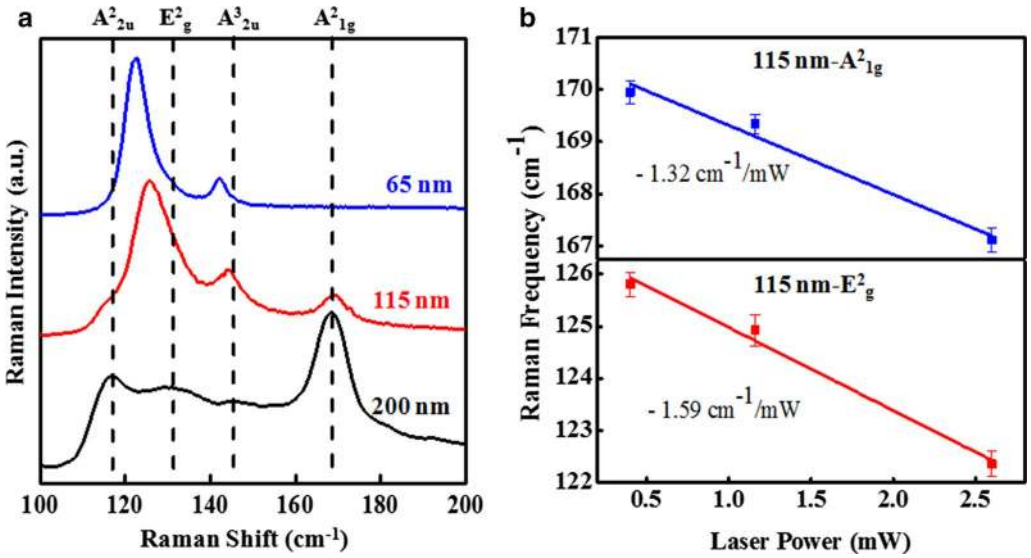


**Fig. 4** **a** Comparison of thickness-dependent micro-Raman spectra of 65-nm, 115-nm and 200-nm $Sb_2Te_3$ flakes at 0.402 mW laser power. The dashed lines show the position of the Raman modes. **b** Raman frequency vs. laser power plots of $E^2_g$ & $A^2_{1g}$ modes for 115-nm $Sb_2Te_3$ flake. The solid lines are the linear fits to the experimental data (symbols). The calculated slopes from the linear fits are shown as insets. The uncertainty in the Raman frequency measurement has been shown as error bars

out-of-plane vibration, which would not be so significant for this thickness.

The Raman spectra comparison of three different thicknesses (65 nm, 115 nm and 200 nm) samples at a particular laser power 0.402 mW is presented in Fig. 4a. All the observed Raman modes and their assignments are listed in Table 1. It is very interesting to observe that $A^2_{1g}$ and $A^2_{2u}$ modes for 200-nm flake possess more intensity than the other two modes ($E^2_g$ and $A^3_{2u}$). $A^2_{1g}$ and $A^2_{2u}$ modes are more sensitive to the thickness because it reflects out-of-plane vibrations and the inter layer van der Walls

**Table1 Positions of Raman modes ($A^2_{2u}$, $E^2_g$, $A^2_{1g}$ and $A^3_{2u}$) of three different $Sb_2Te_3$ flakes (65 nm, 115 nm and 200 nm) at room temperature with 0.402 mW laser power**

| | $A^2_{2u}$ | $E^2_g$ | $A^3_{2u}$ | $A^2_{1g}$ |
|---|---|---|---|---|
| 65 nm | – | 122.65 | 142.20 | – |
| 115 nm | 115.23 | 125.91 | 144.57 | 169.17 |
| 200 nm | 116.42 | 130.07 | 145.46 | 168.28 |

interactions. In the case of $Sb_2Te_3$ flakes with the thickness of 65 nm and 115 nm, the shape of $E^2_g$ peaks for all laser powers looks asymmetry, which implies that there is a merging of both $A^2_{2u}$ and $E^2_g$ modes. However, the $A^2_{1g}$ is completely absent for $Sb_2Te_3$ flake with the thickness of 65 nm. This particular Raman mode would originate due to out-of-plane vibration, which might be unresponsive for this thickness. A red shift is observed for $E^2_g$ and $A^3_{2u}$ phonon modes in the case of thinner flakes, similar to that reported by Zang et al. [30], whereas $A^2_{1g}$ mode shows a slightly blue shift (see Table 1). The peak intensities of 65-nm $Sb_2Te_3$ flake are found to be more pronounced than thicker ones under the same excitation laser power, and this phenomenon can be attributed to optical interference enhancements occurring for both the excitation laser and the emitted Raman radiation in the layered TI/$SiO_2$/Si system [30], which is also reported for $Bi_2Se_3$ and $Bi_2Te_3$ [26, 31]. From the power-dependent Raman spectra of 115-nm $Sb_2Te_3$ flake (Fig. 3b), the Raman frequencies of $E^2_g$ & $A^2_{1g}$ modes have been extracted as a function of laser power as shown in Fig. 4b. The change in the phonon frequency with change in the incident laser power *i.e.,* power coefficient ($\delta\omega/\delta P$) has been estimated from linear fit to extracted data, which is found to be $-1.59$ $cm^{-1}$/mW and $-1.32$ $cm^{-1}$/mW corresponding to $E^2_g$ and $A^2_{1g}$ modes.

The temperature-dependent Raman spectra were measured in the temperature range from 100 to 300 K as shown in Fig. 5 for three different flakes with the thicknesses 80 nm, 115 nm and 400 nm, respectively, at 1.16 mW laser power. The OM, AFM images along with height profiles of 80-nm and 400-nm exfoliated $Sb_2Te_3$ flakes are given in Additional file 1: supporting information S1. At the lower temperature of 100 K, four characteristics Raman modes ($A^2_{2u}$, $E^2_g$, $A^2_{1g}$ and $A^3_{2u}$) of $Sb_2Te_3$ are clearly distinguishable, whereas $A^2_{2u}$ and $E^2_g$ Raman modes get merge together toward higher temperatures *i.e.,* 220 K and 300 K. Red shift and peak broadening were observed all the Raman modes ($A^2_{2u}$, $E^2_g$, $A^2_{1g}$ and $A^3_{2u}$) with the increase in temperature from 100 to 300 K. In general, temperature-dependent Raman spectroscopy is widely used to investigate the thermal expansion, thermal conduction and interlayer coupling [15, 31, 32]. In addition, the peak frequency has a linear dependence with the temperature, which is given by [15],

$$\omega(T) = \omega_0 + \chi T \tag{1}$$

where $\omega_0$ is the frequency of vibration of these phonon modes at absolute zero temperature, and $\chi$ is the first-order temperature coefficient of these phonon modes. It has been reported that thermal expansion and contraction of the crystal and phonon modes may lead to the dependency of the peak position in Raman spectroscopy with temperature [33].

The peak position versus temperature plots of $E^2_g$ & $A^2_{1g}$ modes are shown in Fig. 6a, b, respectively, for different thickness samples. The peak position versus temperature plots (Fig. 6a, b) have been linearly fitted using Eq. 1 to calculate the first-order temperature coefficient ($\chi$), and the values of first-order temperature coefficient for $E^2_g$ & $A^2_{1g}$ Raman modes are listed in Table 2. The broadening in *FWHMs* of $E^2_g$ & $A^2_{1g}$ Raman modes with increase of the temperature is shown in Fig. 7a, b, respectively. The temperature dependence of the *FWHM* is a measure of phonon anharmonicity, and it increases linearly with increase in temperature. The simplest anharmonic approximation, known as the symmetrical three phonon coupling model [34], takes into account the optical phonon decay into two phonons with equal energies and opposite momenta. In the present work, we

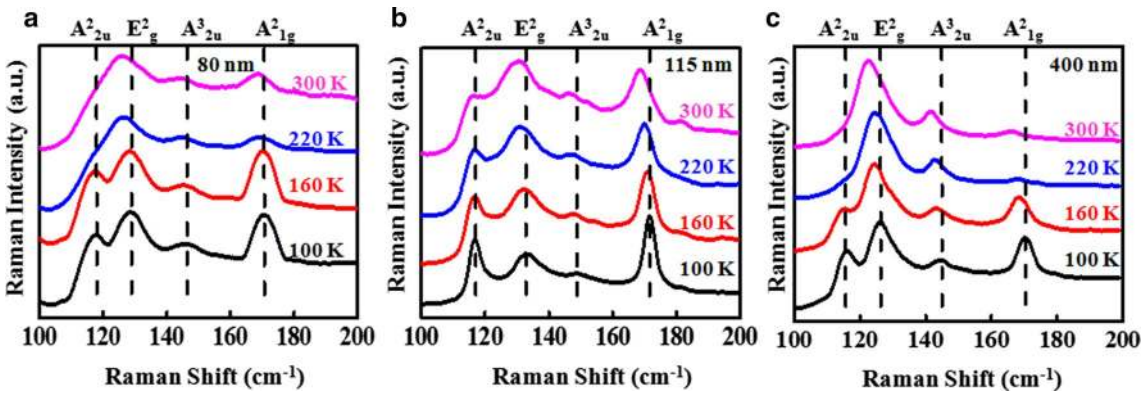


**Fig. 5** **a-c** Temperature-dependent micro-Raman spectra of $Sb_2Te_3$ of thickness 80 nm, 115 nm and 400 nm, respectively. The black-, red-, blue- and light blue-colored curves represent the Raman spectra at 100 K, 160 K, 220 K and 300 K, respectively, for 1.16 mW laser power. The dashed lines show the position of the Raman modes.

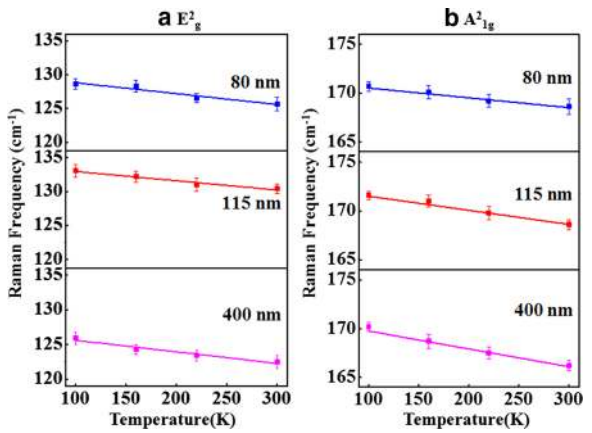


**Fig. 6** Raman frequency vs. temperature plots of **a** $E^2_g$ mode and **b** $A^2_{1g}$ mode for 80-nm, 115-nm and 400-nm $Sb_2Te_3$ flakes. The solid lines are the linear fits to the experimental data (symbols). The uncertainty in the Raman frequency measurement has been shown as error bars

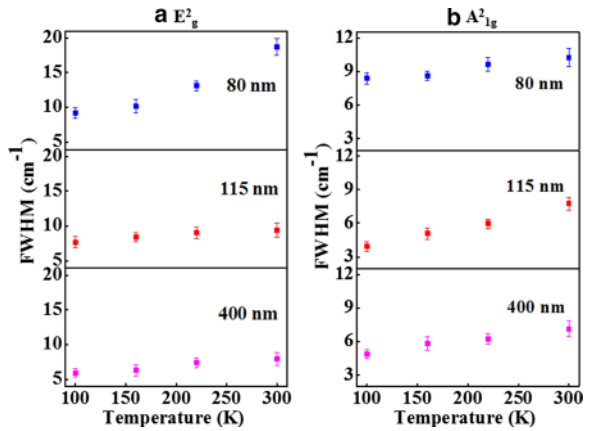


**Fig. 7** FWHM vs. temperature plots of **a** $E^2_g$ mode and **b** $A^2_{1g}$ mode for 80-nm, 115-nm and 400-nm $Sb_2Te_3$ flakes. The uncertainty in the FWHM estimation has been shown as error bars

**Table 2 The first-order temperature coefficient (χ) for different Raman modes of some 2D thermoelectric materials along with the present work**

| Material | Temperature coefficient ($cm^{-1}$/K) | | | Ref |
|---|---|---|---|---|
| TMDCs | χ- $E^1_{2g}$ | χ- $A_{1g}$ | | |
| $MoS_2$ (single layer) | −0.013 | −0.016 | | [35] |
| $MoS_2$ (few layer) | −0.016 | −0.011 | | [36] |
| $WSe_2$ (single layer) | −0.0048 | −0.0032 | | [37] |
| Trichalcogenides | | χ-$A_{1g}$ | χ-$A_{2g}$ | |
| $TiS_3$ nanoribbons | | −0.018 | −0.021 | [38] |
| $TiS_3$ nanosheets | | −0.02 | −0.024 | [38] |
| TIs | χ-$A^1_{1g}$ | χ-$E^2_g$ | χ-$A^2_{1g}$ | |
| $Bi_2Se_3$ nanoplates | −0.01258 | −0.01385 | −0.02363 | [15] |
| $Bi_2Te_3$ nanowires | | | −0.0128 | [39] |
| $Sb_2Te_3$ (400 nm) | | −0.016 | −0.018 | This work |
| $Sb_2Te_3$ (115 nm) | | −0.014 | −0.015 | This work |
| $Sb_2Te_3$ (80 nm) | | −0.016 | −0.01 | This work |

have calculated the first-order temperature coefficient ($\chi$) and thermal conductivity from temperature-dependent Raman spectra. However, we are not analyzing the *FWHM* in the context of *ZT* as it has no such direct relevance to it.

It is observed that the value of first-order temperature coefficients ($\chi$) for $E^2_g$ and $A^2_{1g}$ mode is in order of $10^{-2}$ $cm^{-1}$/K. The value of $\chi$ corresponding to $A^2_{1g}$ mode decreases from $-2\times10^{-2}$ to $-1\times10^{-2}$ $cm^{-1}$/K when the thickness of $Sb_2Te_3$ flake is reduced from 400 to 80 nm. Such low $\chi$ would give low thermal conductivity and favor to get a high figure of merit (*ZT*). However, the value of $\chi$ corresponding to $E^2_g$ mode is almost constant and is independent of thickness. Now, we have calculated an approximate value of thermal conductivity of $Sb_2Te_3$ flake using the power coefficient and first-order temperature coefficient values. The heat conduction through a surface with the cross-sectional area *S* can be evaluated from the following equation: $\partial Q/\partial t = -\kappa \oint \nabla T.dS$, where *Q* is the amount of heat transferred over the time *t* and *T* is the absolute temperature. Considering the radial heat flow, Balandin et al. [40] have derived an expression for thermal conductivity of graphene, which is given by

$$= (1/2\pi h)(\Delta P/\Delta T) \tag{2}$$

where *h* is the thickness of the 2D film of the material and the local temperature rise $\Delta T$ is due to the change in heating power $\Delta P$. By differentiating Eq. (1) with respect to power and substituting ($\Delta P/\Delta T$) in expression (2), the thermal conductivity can be written as follows,

$$= \chi\left(\frac{1}{2\pi h}\right)\left(\frac{\delta\omega}{\delta P}\right)^{-1} \tag{3}$$

where $\kappa$ is thermal conductivity, *h* is the thickness of the 2D film of the material, $\chi$ is the first-order temperature coefficient, and ($\delta\omega/\delta P$) is change in the phonon frequency with change in the incident laser power *i.e.,* power coefficient of particular Raman modes. The calculated thermal conductivity is found to be ~ 10 W/m–K for $Sb_2Te_3$ flake with the thickness of 115 nm supported on 300-nm $SiO_2$/ Si substrate. This value is relatively higher than the reported thermal conductivity of other TI [41]. The slight enhancement in thermal conductivity suggests that the supporting substrate plays a more sensitive role

*i.e.,* the value of thermal conductivity might be dependent on interfacial charges [42]. This higher thermal conductivity at the substrate-supported sample can also explain the smaller temperature rise under high laser power in comparison with the suspended sample. The similar substrate effect is also reported in Su et al. for black phosphorus layers [42]. Guo et al. also reported that, in certain regions, the effect of phonon scattering can be suppressed and the thermal conductivity of nanomaterials can be surprisingly increased due to the coupling induced shift of phonon band to the low wave vector [43]. Recently, a theoretical study on the substrate effect of the thermal conductivity of graphene has been also reported. The authors also found that both the reduction and the increment of thermal conductivity can be induced by the substrate, depending on the coupling condition [44]. From Eq. 3, thermal conductivity is directly proportional to the first-order temperature coefficient, and it is well known that figure of merit (*ZT*) is inversely proportional to the thermal conductivity. Hence, low $\chi$ and $\kappa$ are promising to achieve high *ZT*.

Further work is in the process to achieve $Sb_2Te_3$ nanoflake with thickness less than 7 QL, which is the confinement limit of 2D TI using exfoliation technique with help of special-type scotch tape or by using chemical vapor deposition. Such low thickness flakes are expected to yield a very low-temperature coefficient ($\sim 10^{-3}$ to $10^{-4}$ $cm^{-1}/K$) and a high *ZT*. With high *ZT*, 2D $Sb_2Te_3$ would have great potential in the field of thermoelectric applications.

## Conclusions

In conclusion, we have successfully synthesized 2D $Sb_2Te_3$ of various thicknesses in the range of 65–400 nm using mechanical exfoliation and studied the thermometry of these nanoflakes. The temperature dependence of the peak position and line width of phonon modes $A^2_{1g}$ and $E^2_g$ modes were analyzed to determine the temperature coefficient, which is found to be in the order of $10^{-2}$ $cm^{-1}/K$. The temperature coefficient in the out-of-plane direction decreases with decrease in $Sb_2Te_3$ thickness. Such a low-temperature coefficient would favor to achieve a high *ZT* and pave the way to use this material as excellent candidates of thermoelectric materials. Using temperature coefficient and power coefficient values, the thermal conductivity of 115-nm $Sb_2Te_3$ flake supported on 300-nm $SiO_2$/ Si substrate was estimated to be ~ 10 W/m–K. The slightly higher thermal conductivity compared to other TIs suggests that the supporting substrate significantly affects the heat dissipation of the $Sb_2Te_3$ flake.

## Supplementary information

The online version contains supplementary material available at https://doi.org/10.1186/s11671-020-03463-1.

**Additional file 1.** The supplementary material contains the optical images & AFM images along with heightprofiles of 80-nm and 400-nm exfoliated Sb2Te3 flakes and Raman peak of silicon at 520.74cm-1.

### Abbreviations

TIs: Topological insulators; *ZT*: Figure of merit; OM: Optical micrograph; AFM: Atomic force microscopy; *FWHM*: Full width at half maximum; QL: Quintuple layer.

### Acknowledgements

P.K.N. acknowledges the financial support from Department of Science and Technology, Government of India (DST-GoI), with sanction Order No. SB/S2/RJN-043/2017 under Ramanujan Fellowship. This work was partially supported by DST-GoI that led to the establishment of Nano Functional Materials Technology Centre (NFMTC) (SR/NM/NAT/02—2005 and DST/NM/JIIT-01/2016 (C)).

### Authors' contributions

M.P.S. performed the experiments and analyzed the data. M.M. helped in analyzing the data. M.P.S., M.M. and P.K.N. wrote the manuscript. All the authors took part in the discussion and approved the content of the work. P.K.N supervised the whole project. All authors read and approved the final manuscript.

### Funding

This research is supported by Department of Science and Technology, India, with sanction Order No. SB/S2/RJN-043/2017 under Ramanujan Fellowship.

### Availability of data and materials

The data that support the findings of this study are available from the corresponding author upon reasonable request.

### Competing interests

The authors declare that they have no competing interests.

### Author details

[1] Department of Physics and Materials Science Research Centre, Indian Institute of Technology Madras, Chennai 600 036, India. [2] Department of Physics, Indian Institute of Technology Madras, Chennai 600 036, India. [3] Nano Functional Materials Technology Centre, Indian Institute of Technology Madras, Chennai 600 036, India.

Received: 28 July 2020 Accepted: 11 December 2020
Published online: 03 February 2021

### References

1. Hasan MZ, Kane CL (2010) Colloquium: topological insulators. Rev Mod Phys 82:3045
2. Xia Y, Qian D, Hsieh D, Wray L, Pal A, Lin H et al (2009) Observation of a large-gap topological-insulator class with a single Dirac cone on the surface. Nature Phys 5:398
3. Checkelsky JG, Hor YS, Cava RJ, Ong NP (2011) Bulk band gap and surface state conduction observed in voltage-tuned crystals of the topological insulator $Bi_2Se_3$. Phys Rev Lett 106:196801
4. Chen J, Qin HJ, Yang F, Liu J, Guan T, Qu FM et al (2010) Gate-voltage control of chemical potential and weak anti-localization in bismuth selenide. Phys Rev Lett 105:176602
5. Steinberg H, Gardner DR, Lee YS, Jarillo-Herrero P (2010) Surface state transport and ambipolar electric field effect in $Bi_2Se_3$ nanodevices. Nano Lett 10:5032
6. Zhang X, Wang J, Zhang SC (2010) Topological insulators for high-performance terahertz to infrared applications. Phys Rev B 82:245107
7. Qi XL, Hughes TL, Zhang SC (2008) Topological field theory of time-reversal invariant insulators. Phys Rev B 78:195424

8. Essin AM, Moore JE, Vanderbilt D (2009) Erratum: magnetoelectric polarizability and axion electrodynamics in crystalline insulators. Phys Rev Lett 103:259902
9. Osterhage H, Gooth J, Hamdou B, Gwozdz P, Zierold R, Nielsch K (2014) Thermoelectric properties of topological insulator $Bi_2Te_3$, $Sb_2Te_3$, and $Bi_2Se_3$ thin film quantum wells. Appl Phys Lett 105:123117
10. Guo M, Wang Z, Xu Y, Huang H, Zang Y, Liu C et al (2016) Tuning thermoelectricity in a $Bi_2Se_3$ topological insulator via varied film thickness. New J Phys 18:015008
11. Tan G, Zhao LD, Shi F, Doak JW, Lo SH, Sun H et al (2014) High thermoelectric performance of p-type SnTe via a synergistic band engineering and nanostructuring approach. J Am Chem Soc 136:7006
12. Wei PC, Liao CN, Wu HJ, Yang D, He J, Biesold-McGee GV et al (2020) Thermodynamic routes to ultralow thermal conductivity and high thermoelectric performance. Adv Mater 32:1906457
13. Biswas K, He JQ, Zhang QC, Wang GY, Uher C, Dravid VP et al (2011) Strained endotaxial nanostructures with high thermoelectric figure of merit. Nat Chem 3:160
14. Kim Y, Chen X, Wang Z, Shi J, Miotkowski I, Chen YP et al (2012) Temperature dependence of Raman-active optical phonons in $Bi_2Se_3$and $Sb_2Te_3$. Appl Phys Lett 100:071907
15. Zhou F, Zhao Y, Zhou W, Tang D (2018) Temperature- dependent Raman scattering of large size hexagonal $Bi_2Se_3$ single-crystal nanoplates. Appl Sci 8:1794
16. Rivas N, Zhong S, Dekker T, Cheng M, Gicala P, Chen F et al (2019) Generation and detection of coherent longitudinal acoustic waves in ultrathin 1*T*′-$MoTe_2$. Appl Phys Lett 115:223103
17. Song QJ, Tan QH, Zhang X, Wu JB, Sheng BW, Wan Y et al (2016) Physical origin of Davydov splitting and resonant Raman spectroscopy of Davydov components in multilayer $MoTe_2$. Phys Rev B 93:115409
18. Zhang X, Qiao XF, Shi W, Wu JB, Jiang DS, Tan PH (2015) Phonon and Raman scattering of two-dimensional transition metal dichalcogenides from monolayer, multilayer to bulk material. Chem Soc Rev 44:2757
19. Chen SY, Goldstein T, Venkataraman D, Ramasubramaniam A, Yan J (2016) Activation of new Raman modes by inversion symmetry breaking in type II Weyl semimetal candidate T′-$MoTe_2$. Nano Lett 16:5852
20. Richter W, Kohler H, Becker CR (1977) A Raman and far-infrared investigation of phonons in the rhombohedra1 $V_2$-$VI_3$ compounds $Bi_2Te_3$, $Bi_2Se_3$, $Sb_2Te_3$ and $Bi_2(Te_{1-x}Se_x)_3$ ($0 < x < l$), $(Bi_{1-y}Sb_y)_2Te_3$ ($0 < y < 1$). Phys Status Solidi B 84:619
21. Richter W, Krost A, Nowak U, Anastassakis E (1982) Anisotropy and dispersion of coupled plasmon-LO-phonon modes in $Sb_2Te_3$. Z Phys B Condens Matter 49:191
22. Serrano J, Manjon FJ, Romero AH, Widulle F, Lauck R, Cardona M (2003) Dispersive phonon linewidths: The $E_2$ phonons of ZnO. Phys Rev Lett 90:055510
23. Zhou S, Tao X, Gu Y (2016) Thickness-dependent thermal conductivity of suspended two-dimensional single-crystal $In_2Se_3$ layers grown by chemical vapor deposition. J Phys Chem C 120:4753
24. Sriram P, Manikandan A, Chuang FC, Chueh YL (2020) 2D Transition Metal Dichalcogenides: Hybridizing Plasmonic Materials with 2D-Transition Metal Dichalcogenides toward Functional Applications. Small 16:1904271
25. Shahil KMF, Hossain MZ, Teweldebrhan D, Balandin AA (2010) Crystal symmetry breaking in few-quintuple $Bi_2Te_3$ films: Applications in nanometrology of topological insulators. Appl Phys Lett 96:153103
26. Teweldebrhan D, Goyal V, Balandin AA (2010) Exfoliation and characterization of bismuth telluride atomic quintuples and quasi-two-dimensional crystals. Nano Lett 10:1209
27. Sosso GC, Caravati S, Bernasconi M (2009) Vibrational properties of crystalline $Sb_2Te_3$ from first principles. J Phys: Condens Matter 21:095410
28. Sahoo S, Gaur APS, Ahmadi M, Guinel MJF, Katiyar RS (2013) Temperature-dependent raman studies and thermal conductivity of few-layer $MoS_2$. J Phys Chem C 117:9042
29. Zhang J, Peng Z, Soni A, Zhao Y, Xiong Y, Peng B (2011) Raman spectroscopy of few-quintuple layer topological insulator $Bi_2Se_3$ nanoplatelets. Nano Lett 11:2407
30. Dang W, Peng H, Li H, Wang P, Liu Z (2010) Epitaxial heterostructures of ultrathin topological insulator nanoplate and graphene. Nano Lett 10:2870
31. Xia J, Li XZ, Huang X, Mao N, Zhu DD, Wang L et al (2016) Physical vapor deposition synthesis of two-dimensional orthorhombic SnS flakes with strong angle/temperature-dependent Raman responses. Nanoscale 8:2063
32. Taube A, Lapinska A, Judek J, Zdrojek M (2015) Temperature dependence of Raman shifts in layered $ReSe_2$ and $SnSe_2$ semiconductor nanosheets. Appl Phys Lett 107:013105
33. Luo S, Qi X, Yao H, Ren X, Chen Q, Zhong J (2017) Temperature-dependent raman responses of the vapor-deposited tin selenide ultrathin flakes. J Phys Chem C 121:4674
34. Klemens PG (1966) Anharmonic decay of optical phonons. Phys Rev 148:845
35. Lanzillo NA, Glen Birdwell A, Amani M, Crowne FJ, Shah PB, Najmaei S, Liu Z, Ajayan PM, Lou J, Dubey M, Nayak SK (2013) Temperature-dependent phonon shifts in monolayer MoS2. Appl Phys Lett 103:093102
36. Thripuranthaka M, Kashid RV, Sekhar Rout C, Late DJ (2014) Temperature dependent Raman spectroscopy of chemically derived few layer $MoS_2$ and $WS_2$ nanosheets. Appl Phys Lett 104:081911
37. Late DJ, Shirodkar SN, Waghmare UV, Dravid VP, Rao CN (2014) Thermal expansion, anharmonicity and temperature-dependent Raman spectra of single-and few-layer $MoSe_2$ and $WSe_2$. Chem Phys Chem 15:1592
38. Pawbake AS, Island JO, Flores E, Ares JR, Sanchez C, Ferrer IJ, Jadkar SR, Van Der Zant HS, Castellanos-Gomez A, Late DJ (2015) Temperature-dependent Raman spectroscopy of titanium trisulfide ($TiS_3$) nanoribbons and nanosheets. ACS Appl Mater Interfaces 7:24185
39. Park D, Park S, Jeong K, Jeong HS, Song JY, Cho MH (2016) Thermal and electrical conduction of single-crystal $Bi_2Te_3$ nanostructures grown using a one step process. Sci Rep 6:1
40. Balandin AA, Ghosh S, Bao W, Calizo I, Teweldebrhan D, Miao F, Lau CN (2008) Superior thermal conductivity of single-layer graphene. Nano Lett 8:902
41. Luo Z, Tian J, Huang S, Srinivasan M, Maassen J, Chen YP, Xu X (2018) Large enhancement of thermal conductivity and Lorenz number in topological insulator thin films. ACS Nano 12:1120
42. Su L, Zhang Y (2015) Temperature coefficients of phonon frequencies and thermal conductivity in thin black phosphorus layers. Appl Phys Lett 107:071905
43. Guo ZX, Zhang D, Gong XG (2011) Manipulating thermal conductivity through substrate coupling. Phys Rev B 84:075470
44. Ong ZY, Pop E (2011) Effect of substrate modes on thermal transport in supported graphene. Phys Rev B 84:075471


## Publisher's Note